Optical Waveguiding and Lasing Action in Porphyrin Rectangular Microtube with Subwavelength Wall Thicknesses

Seok Min Yoon,[‡,§,⊥] Jooran Lee,[†,⊥] Jung Ho Je,[§] Hee Cheul Choi,[‡,*] and Minjoong Yoon[†,*]

[†]Molecular/Nano Photochemistry & Photonics Lab, Department of Chemistry, Chungnam National University, 79 Daehak-Ro, Yuseong-gu, Daejeon 305-764, South Korea, [‡]Department of Chemistry and Division of Advanced Materials Science, and [§]X-ray Imaging Center, Department of Materials Science and Engineering, Pohang University of Science & Technology (POSTECH), San 31, Hyoja-Dong, Nam-Gu, Pohang 790-784, South Korea. [⊥] These authors contributed equally to this work.

ABSTRACT Lasing action by planar-, fiber-, or ring-type waveguide has been extensively investigated with different types of microcavities such as thin films, wires, cylindrical tubes, or ribbons. However, the lasing action by sharp bending waveguide, which promises efficient interconnection of amplified light in the photonic circuits, remains unexplored. Here, we report the first observation of microcavity effects in the organic rectangular microtubes (RMTs) with sharp bends (*ca.* 90°) and subwavelength nanoscale wall thicknesses, based on single crystalline and themostable tetra(4-pyridyl)porphyrin (H_2TPyP)-RMTs synthesized by the VCR process. A bright tip emission is observed from the sharp bending edges of a single RMT upon laser excitation, demonstrating a clear waveguiding behavior in RMT. The appearance of a peak from the (0−1) band at a threshold tube length and the gradual decrease of its full width at half-maximum (fwhm) suggest that amplification of spontaneous emission (ASE) is developed by stimulated emission along the walls of the RMTs. The ehancement of the ASE peak together with the narrowing of its fhwm over a threshold pump power and the tube size (width and length) dependence of the mode spacing strongly support vibronic lasing action in the RMTs. The stimulated emission by the subwavelength bending waveguide demonstrates that the organic RMTs can be applied as new building blocks for micromanipulation of optical path and amplification in the integrated circuits for efficient photonic devices.

KEYWORDS: porphyrin · rectangular microtube · sharp bending waveguide · amplified spontaneous emission (ASE) · lasing action · rectangular ring mode

Electrically and optically active organic molecules have been attracting great attention for their potential application as cost-effective and high-performance optoelectronic devices.[1−3] Especially when individual organic unit molecules are self-assembled into one-dimensional (1D) nano- and microstructures, remarkably improved or unprecedented optoelectronic properties are achievable, enabling one to induce stimulated emission by waveguiding in a 1D resonator. It has been demonstrated that low-dimensional organic materials can be applied in laser and photonic circuits due to high interconnectivity between photonic circuit elements, high spectral tunability, and large stimulated emission cross sections.[4−8] For example, individual nanowires of poly(9,9-dioctylfluorene) (PFO)[4] and 2,4,5-triphenylimidazole (TPI)[5] act as cylindrical optical cavities, exhibiting optically pumped lasing under ambient conditions with low threshold energies (∼nJ). Most of the lasing actions in the organic microresonators have been investigated using solid structures such as wires[4,5] or thin films.[9,10] However, no systematic investigation has been carried out on the lasing action in hollow tubular structures, particularly rectangular tubes with sharp bends (*ca.* 90°) and subwavelength-scale wall thicknesses, which might show very different waveguiding behaviors from conventional 1D solid structures.[6,11] Thus, hereby, we attempted to fabricate the organic rectangular microtube waveguides using porphyrins.

Porphyrin nano/microstructures have been attracting much interest in their electrical and optical properties for optoelectronic applications,[12,13] but they have not been applied to lasing and waveguides. This motivated us to synthesize well-defined single crystalline porphyrin nano/microstructures for their application to desirable optoelectronic devices including lasers. Recently, we successfully applied the varporization−condensation−recrystallization (VCR) process[14−18] to synthesize rectangular nanotubes (RNTs) of 5,10,15,20-tetra(4-pyridyl)-porphyrin (H_2TPyP).[14] Hence, we synthesized the rectangular microtubes (RMTs) of H_2TPyP (H_2TPyP-RMTs) by the VCR process through modification of the flow rate of Ar carrier gas to be slower than that for the synthesis of RNTs,[14] and we investigated their optical

* Address correspondence to mjyoon@cnu.ac.kr, choihc@postech.edu.

Received for review December 21, 2010 and accepted March 10, 2011.

Published online March 10, 2011
10.1021/nn200027x

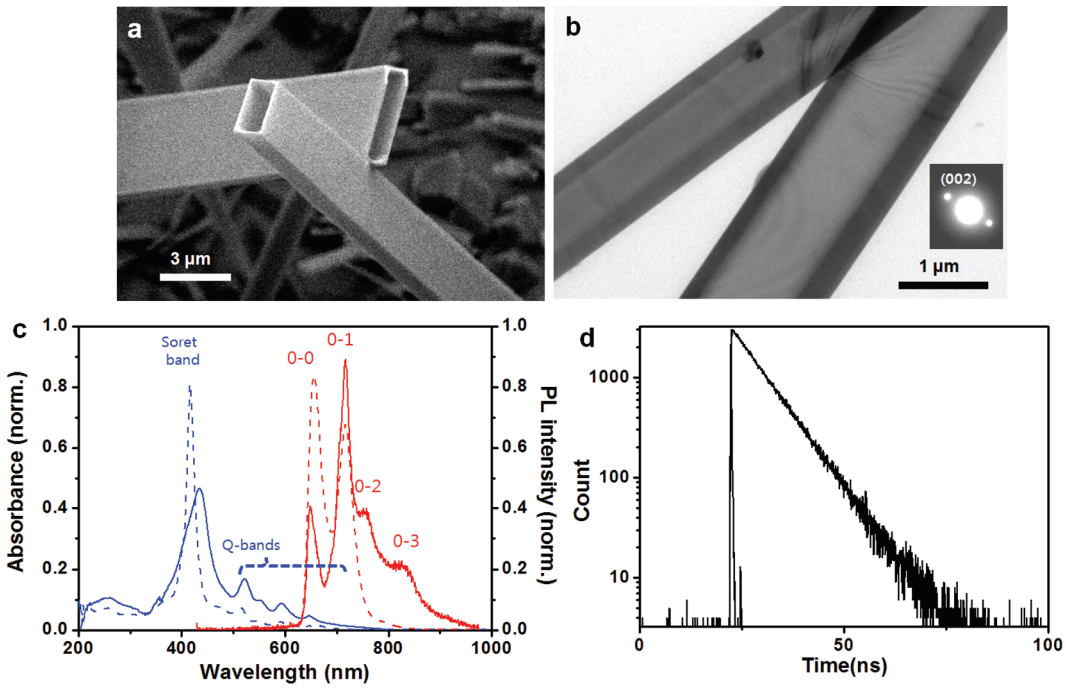

Figure 1. (a) SEM and (b) TEM images of H_2TPyP-RMTs. Inset image of (b) is a selected area electron diffraction (SAED) pattern obtained from the H_2TPyP-RMT on (100) zone plane. (c) Ensemble-averaged absorption (blue dashed line) and photoluminescence (PL, red dashed line, λ_{ex} = 410 nm) spectra from H_2TPyP molecules in chloroform (<10^{-5} M, dotted lines) and from H_2TPyP-RMTs coated on a glass (solid lines). (d) Time-resolved PL spectra of a single H_2TPyP-RMT from the 0−1 band by confocal scanning microscope (CSM)-coupled PL system.

characteristics including high photoluminescence (PL) on the ensemble-averaged and single microtube basis. The H_2TPyP-RMTs were identified to be highly crystalline and thermostable, and their individual RMTs exhibited amplified spontaneous emission (ASE) for lasing action resulting from subwavelength bending waveguide.

RESULTS AND DISCUSSION

The formation of the H_2TPyP-RMTs was initiated by placing H_2TPyP powders in the center of a horizontal heating furnace heated at 450 °C in Ar gas atmosphere. The H_2TPyP-RMTs were readily formed after 30 min on a Si(100) substrate placed at the end region of the furnace where temperature was naturally cooled to 350 °C as in the case of H_2TPyP-RNTs.[14] For the synthesis of high-yield H_2TPyP-RMTs, the flow rate of Ar gas was set up to be 80 sccm.

The as-prepared H_2TPyP-RMTs were clearly identified to have the hollow tubular structures of the rectangular microtubes (Figure 1a,b). In addition, the selected area electron diffraction (SAED) pattern of the H_2TPyP-RMT (inset image of Figure 1b) is the same as that of H_2TPyP-RNTs on (100) zone plane,[14] indicating that the RMT is a well-defined single crystal. The width, height, and wall thickness of the RMTs were *ca.* 0.5−5, 0.25−2, and 0.05−0.4 μm, respectively. The lengths mostly exceeded 10 μm. The H_2TPyP-RMTs were found to be thermally stable single crystals as approved by observation of their thermal decomposition temperature at 450 °C by thermogravimetric analysis.[14] The detail structure of a H_2TPyP-RMT was characterized by analysis of the data obtained from SAED patterns and X-ray single crystallography of a H_2TPyP-RMT having 20 μm in width length and 5 μm in height examined by using a synchrotron X-ray beam source, confirming that it was self-assembled by hydrogen−π, π−π, and hydrogen bonding intermolecular interactions as reported.[14]

Ensemble-averaged optical properties of the crystalline H_2TPyP-RMTs were investigated by using a UV−vis spectrophotometer and conventional photoluminescence (PL) spectrophotometer. UV−vis absorption (blue line) and PL emission (red line) spectra (Figure 1c) were obtained from a chloroform solution of H_2TPyP (dotted line) and a random mat of H_2TPyP-RMTs coated on a glass (solid line). The absorption spectrum of the solution exhibits a sharp Soret band at 417 nm along with Q-bands beyond 480 nm, which is a characteristic spectrum of porphyrin monomers. On the other hand, the bands in the absorption spectrum of the random RMT mat are considerably red-shifted and broadened with enhanced Q-bands as compared with those of the absorption spectrum of the monomers, implying that *J*-aggregation through π−π intermolecular interactions of H_2TPyP is responsible for the formation of RMTs.[14,19] The PL spectrum of the H_2TPyP solution exhibits two vibronic emission bands at 655 and 716 nm originated from the 0−0 and 0−1 vibronic transitions in the electronic transition $S_1 \rightarrow S_0$, respectively. In the random solid RMT mat, however, the

intensity of the 0−0 vibronic band significantly decreases, while the 0−1 band increases with enhanced vibronic structural bands at ~760 and ~830 nm originated from 0−2 and 0−3 vibronic transition, respectively, suggesting a narrowed distribution of emitting RMT segments with increased effective conjugation due to the *J*-aggregation. The long wavelength tail beyond 860 nm is attributed to unresolved vibronic replicas. The decrease of the 0−0 vibronic band is ascribed to the self-absorption of the emitted PL due to the concentrated *J*-aggregation, as supported by the enhanced absorption of Q-bands of which the wavelengths are well overlapped with the ones of emitted PL. The self-absorption of PL emission implies that the overall excitation energy is well conserved without loss in the structures of H_2TPyP-RMTs. Such minimized excitation energy loss can enhance the 0−1 emission at the expense of quenching of 0−0 emission, keeping the high PL quantum yield of H_2TPyP-RMTs (Φ_f = 0.267), much higher than that of standard tetraphenyl porphyrin (Φ_{sf} = 0.099).[20,21] In parallel with the high quantum yield, the PL emission decay time was very long at 7.6 ns (Figure 1d), as measured from a single H_2TPyP-RMT for the 0−1 emission band. It is also noteworthy that there exists only one single PL decay component. These results imply that the crystallinity of the H_2TPyP-RMTs is very high.

Optical properties of individual H_2TPyP-RMTs were also examined by using a CSM-coupled PL system (Figure S1 in Supporting Information). Figure 2a,b shows bright-field (BF) and epi-PL micrographs of individual H_2TPyP-RMTs on another random mat of glass substrate, exhibiting characteristic red emission. Interestingly, the emission from the tube tips is significantly brighter than that from the bodies upon wide-field excitation at 415 nm, indicating that the PL emission waves are guided along the RMT growth axis (*b*-axis). Such a waveguide behavior was observed from more than 60% of the individual RMTs on the random mats investigated. The detailed optical waveguiding properties of the RMTs were investigated with a representative single RMT (30.7 μm length, 2.17 μm width, 250 nm wall thickness) (Figure 2c) by measuring the CSM-coupled PL images (Figure 2d−i). As can be seen in the epi-PL image (Figure 2d), the wall of RMT clearly exhibited brighter emission than the hollow region, indicating the confinement of PL emission wave in the walls. In addition, both end tips of the tube are always much brighter than the body wall regardless of the laser beam position along the tube (Figure 2e−g). Also, the tip closed to the laser beam was gleamed with brighter emission than the other tip (Figure 2f,g). These observations support the behavior of typical waveguides[5,6] of the H_2TPyP-RMTs. Another important feature is that the bright tip emission was generated from the sharp bending (90°) edges of the cross section of a tilted single RMT (20 μm length, 1.69 μm width) as shown in Figure 2i, indicating minimized optical loss in the waveguiding process. The waveguide behavior of the RMT is remarkable, when considering the wall thicknesses of 350 nm with the sharp bending edges (*ca.* 90°), which may give rise to large optical loss.[22,23] This may be due to formation of an evanescent wave field on highly crystalline planar dielectric boundaries of the H_2TPyP-RMTs as in the case of other thin slabs.[24−26] Such active waveguide behavior with high optical confinement suggests that H_2TPyP-RMTs can be lasing microresonators.

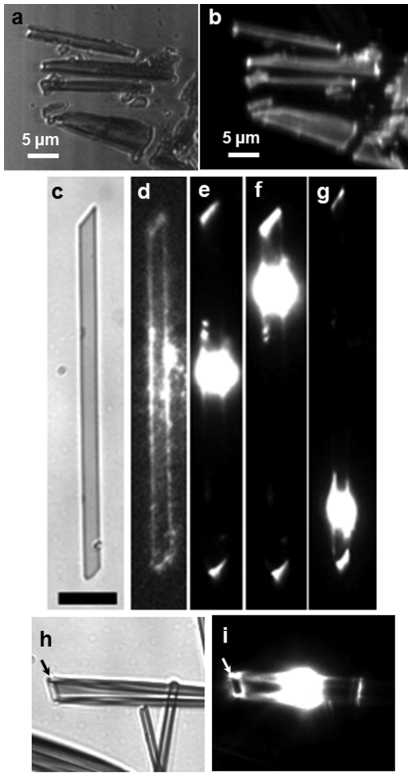

Figure 2. (a) Wide range bright-field (BF) image and (b) epi-PL image of H_2TPyP-RMTs on glass. (c) BF image, (d) epi-PL, and (e−g) PL images of a single H_2TPyP-RMT with 30.7 μm length, 2.11 μm width, and 250 nm wall thickness, taken by focused beam through CSM. The brightest spots in panels e−g and i are excitation laser beams. All images were captured as gray scale mode. (h) BF image and (i) PL image of a tilted single H_2TPyP-RMT with 20 μm length, 1.69 μm width, and 350 nm wall thickness. The arrows in panels h and i indicate the cross-section image of RMT.

As the waveguide and lasing actions are dependent on the size or geometry of the microresonator, the PL emission spectra of the individual tube would be also rely on the tube size, including length, width, and wall thickness as well-known electron-confined three-dimensional box-size dependency on the electronic transition energy. Thus, the size-dependent PL emission spectra were measured from the tip of individual H_2TPyP-RMTs of variable tube length with 1 μm width at a constant laser power of 70 nJ. As shown in Figure 3, the vibronic emission bands were observed to be red-shifted significantly to 732 nm as the tube length

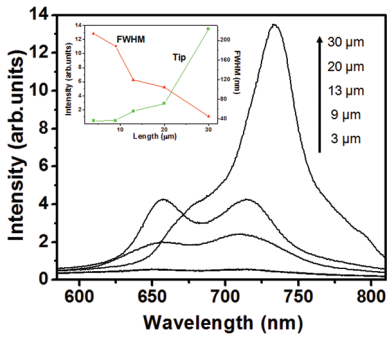

Figure 3. Tube length dependence of the PL spectra collected at 70 nJ excitation power from the tip of single H_2TPyP-RMTs with 1 μm of width. The inset graph shows length dependence of the fwhm (red) and the intensity (green) of the (0−1) emission band measured from the tip.

increased to 30 from 3 μm. This must be due to an increase of effective conjugation length as mentioned above. Interestingly, intensity of the vibronic emission bands were also observed to increase as the tube length increases. Especially, the 0−1 emission band measured from the tip of 30 μm long RMT abruptly increased with its narrowing full width at half-maximum (fwhm), as seen in the inset of Figure 3, whereas the body emission intensity remained relatively low without the abrupt increase of the 0−1 band (data not shown). The tube length dependence of the abrupt increase of the tip emission with the decrease of the fwhm can be ascribed to the amplification of spontaneous emission (ASE) as the ASE is known to be supported by the stripe length dependence of the emission intensity from the thin film of a conjugated polymer[9,10,27] or nanocrystal quantum dot solid,[28] as the intensity of tip emission ($I(\lambda)$) is given by the equation, $I(\lambda) = A(\lambda)I_p/g(\lambda)(e^{g((\lambda)l} - 1)$, where $A(\lambda)$ is a constant related to the cross section for spontaneous emission, I_p is the pump intensity, $g(\lambda)$ is the net gain coefficient, and l is the length of wire. The tube-length-dependent increase of emission intensity is presumably accomplished by stimulated emission during the travel of the spontaneously emitted light along the waveguide, as reported in light emitting polymer thin films.[9,10,28] It is known that the waveguided light in thin slab resonators is polarized above the ASE threshold length to be preferentially stimulated along the thin slabs.[9,10,28] Thus, the observations of the ASE threshold and waveguiding behavior from the H_2TPyP-RMTs consisted with four thin slab-like walls imply that ASE is developed by stimulated emission along the walls of RMTs. Furthermore, the occurrence of the ASE at a higher vibronic (0−1) band rather than (0−0) band indicates that the efficient vibronic lasing action can be operated in the RMT because optical pumping efficiently provides population inversion to form metastable intermediate states.

In order to investigate the stimulated emission behavior of individual RMTs, the emission spectra of a H_2TPyP-RMT (27 μm length and 2 μm and 160 nm wall thickness) were collected from both the tip and the body at various excitation pump powers as shown in Figure 4a and Figure S2 in Supporting Information, respectively. At lower laser powers up to 119 nJ, the vibronic 0−0 emission band of the tip is stronger than the 0−1 band, as illustrated in Figure 4a and Figure S3, in contrast to the ensemble-averaged spectra of the RMT solid mat in Figure 1c. This may be because the self-absorption of the spontaneous emission from the 0−0 vibronic state is smaller in the tip than in the bulk mat at such lower pump powers. It is also conceivable that the PL intensities of the 0−0 and 0−1 bands from the tip linearly increase in the low pump power range (32−119 nJ). However, as the pump power further increases to 149 and 200 nJ, intensity of the 0−1 band steeply enhances and the fwhm narrows down to 6 nm. This indicates the existence of a threshold pump power around 119 nJ (3.4 mJ cm^{-2}), as illustrated in Figure 4b for the 0−1 emission band. Such threshold pump power was not observed from the body emission (Figure 4b and Figure S2), supporting that the stimulated emission is developed in the RMTs as the light travels along the tube to the tip. This suggests that the single H_2TPyP-RMT can act as a rectangular microtube resonator which causes the optically pumped vibronic lasing action, even though the 0−1 band with 6 nm fwhm at the tip is more or less broad as a single mode lasing band. The broad fwhm may be due to multimode lasing, which was not resolved under the wide dispersion measurement condition. Supporting this speculation, the narrow dispersion PL measurement exhibited two mode peaks narrowing into ~1 nm of fwhm as the excitation power increases, as shown in Figure 4c, which are superimposed on the broader ASE peak as the pump power increased. The stimulated emission cross section (σ) of H_2TPyP-RMTs was estimated to be $\sim 7.6 \times 10^{-14}$ cm^2 by using the equation, $\sigma = \lambda^2 g(\lambda)/8\pi n^2 \tau$, with $g(\lambda) = \lambda^2 f(\lambda)/c$, where $f(\lambda)$ is the PL quantum distribution and found to be ~3760 cm^{-1} by area normalizing the PL spectrum of Figure 4a to the PL quantum yield (0.27, *vide supra*), λ = 732 nm, τ (PL lifetime) = 7.6 ns (*vide supra*), and $n \sim 2.1$.[29] This value is relatively larger than that of polycrystalline organic conjugated polymer nanowires ($\sim 5.0 \times 10^{-16}$ cm^2), indicating reduction of the optical loss in single crystalline H_2TPyP-RMTs. This may be due to formation of the evanescent waves on the planar surface boundaries of the RMTs as mentioned above.

Carefully examining the 0−1 and 0−2 stimulated emission bands of a representative RMT with ~700 nm widths, we observed the development of periodic oscillations with increasing the excitation laser power, as illustrated in Figure 5a. This supports the possible coherent emission wave modes characteristic of lasing action. Interestingly, the mode spacing (closed squares in Figure 5b), measured from the 0−1 band, is linearly

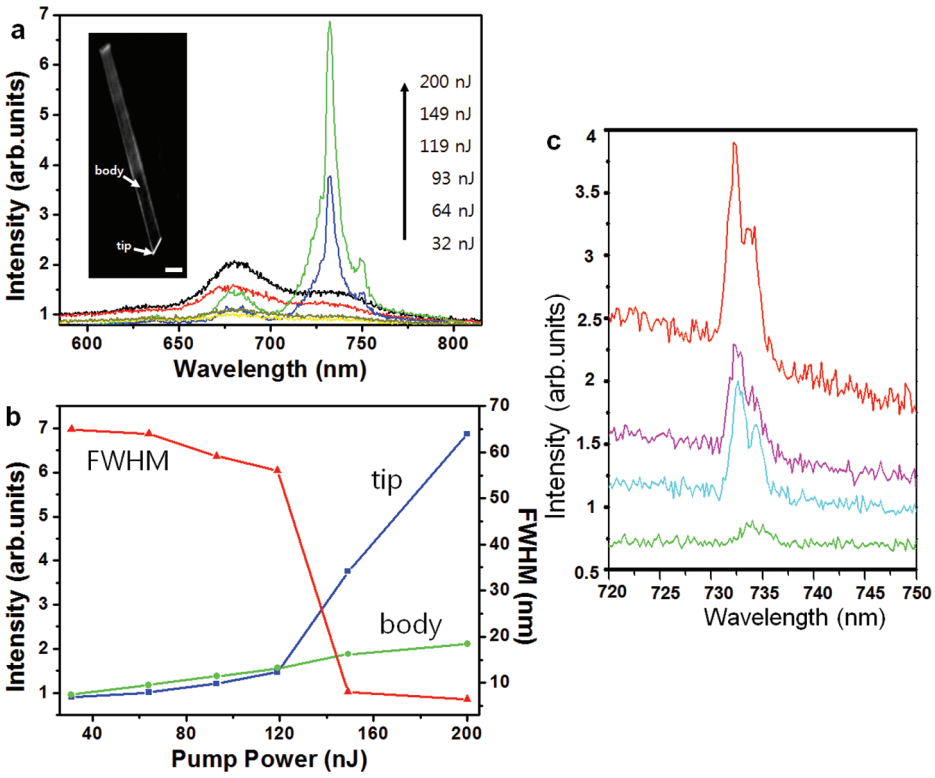

Figure 4. (a) PL spectra collected from the tip of a single H_2TPyP-RMT (27 μm length and 2 μm width (inset PL image)) as a function of excitation pump power. The arrow represents the increase of the excitation pump power from the bottom to top. (b) Plot of the intensity (blue) and the fwhm (red) of 0−1 emission band (732 nm) *vs* pump power. In comparison, the intensity of the body emission (green) is low and weakly increased with pump power. (c) Narrow dispersion PL spectra of a single H_2TpyP-RMT with longer length than 21.5 and 0.7 μm width upon increasing pumping power from 10 (bottom), 90, 130, to 200 nJ (top).

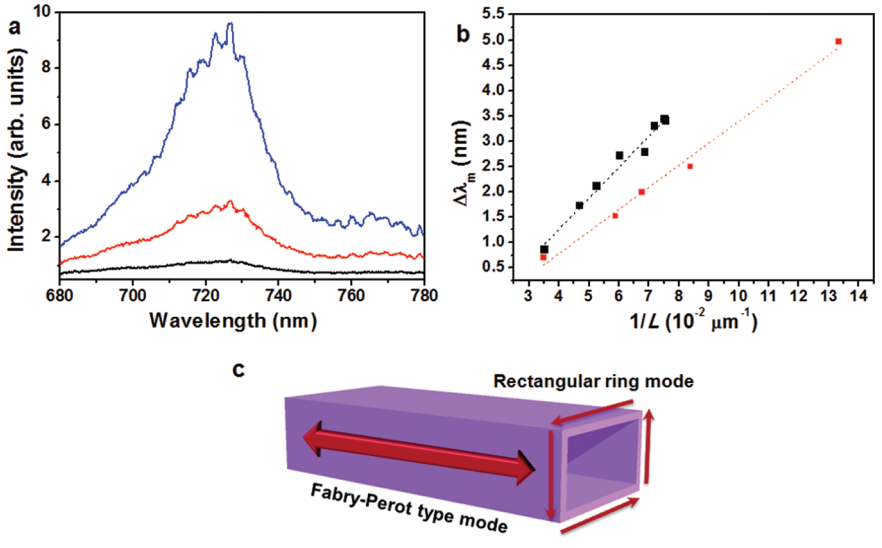

Figure 5. (a) Periodic mode peaks observed on the 0−1 and the 0−2 emission bands of H_2TPyP-RMT with 13.2 μm length and 700 nm width. The spectra were obtained with excitation pump powers from 60 (bottom), 100, to 150 nJ (top). (b) Mode spacing from the (0−1) band plotted with the inverse of the stripe length (1/*L*) of H_2TPyP-RMTs for 700 nm (black) and 1.3 μm (red) widths. (c) Schematic diagram of the waveguide modes in the RMT.

proportional to 1/*L*, as shown in Figure 5b. This clearly implies the occurrence of coherent emission in the RMTs, that is, the stimulated emission. As illustrated by the black squares and dashed line in Figure 5b, the dependence of the mode spacing for the RMTs with ~700 nm width on the tube length was well matched with the Fabry−Perot equation $\Delta\lambda \sim \lambda^2/2L[n - \lambda(dn/d\lambda)]$, where n is refractive index, L is the stripe path length of the guided wave (λ), and $dn/d\lambda$ is the dispersion relation. From this plot, $[n - \lambda(dn/d\lambda)]$ was

determined to be ~5.9, which gives negative and significantly smaller $\lambda(dn/d\lambda)$ than that of π-conjugated polymer nanowires[4] due to the relatively large Stokes shift in the proximity of the absorption edge. This suggests that the tube resonator is primarily operated by Fabry−Perot-type mode along the thin slabs consisting of the RMT.[4,5,25,30−32] Incidentally, it is noteworthy that the mode spacing for RMTs with a bigger width of 1.3 μm (red squares and dashed line in Figure 5b) dropped from that for RMTs with the smaller width (black squares and dashed line in Figure 5b). The drop of the spacing is presumably due to the increase in the total optical path length, indicating that not only the tube length but also the perimeter of RMTs might play an important role in resonating for the lasing action. We thus suggest that combination of two kinds of cavity mode steers the lasing action in a single H_2TPyP-RMT; one is the Fabry−Perot mode to resonate along the growth direction of the tube, and the other is the rectangular ring mode to resonate by wave guiding alongside sharp bending corners,[23,24,26,33,34] as shown in Figure 5c.

In summary, the single crystalline tube structure of H_2TPyP-RMTs with high PL quantum yield and long lifetime drew us to investigate the nature of hollow rectangular optical microresonator. Existence of (1) resonator structure as a RMT, (2) explicit optical threshold pump power for sharpening the higher vibronic bands, and (3) dependence of the mode spacing on both tube length and width suggests that H_2TPyP-RMTs exhibit vibronic lasing action by evanescent wave propagation along the highly crystalline planar dielectric boundaries of four walls. Moreover, the stimulated emission by the subwavelength rectangular waveguiding denotes that RMT can be applied as a nano/microphotonic circuit element not only sharply changing the direction of wave propagation but also emitting amplified optical signal. Considering the potent versatility and tunability of electronic and optical characteristics of the nonmetalloporphyrins by simple postchemical treatments such as an ion exchange process[35,36] or cocrystallization with functional compounds,[37] the H_2TPyP-RMTs would provide a great opportunity to develop future submicrometer-sized organic microphotonic systems.

METHODS

Synthesis and Characterization of 5,10,15,20-Tetra(4-pyridyl)porphyrin Rectangular Microtubes of H_2TPyP (H_2TPyP-RMTs). The rectangular microtubes (RMTs) of H_2TPyP (H_2TPyP-RMTs) were synthesized by a varporization−condensation−recrystallization (VCR) process.[14−18] 5,10,15,20-Tetra(4-pyridyl)porphyrin (H_2TPyP, 0.04 g, 97%) purchased from Sigma-Aldrich was placed in the middle of quartz tube, and solid substrates Si(100) at the end region of the quartz tube were located in a horizontal electrical heating furnace. Prior to reactions, the inner atmosphere of the horizontal quartz tube was fluently flushed out with pure Ar gas (99.999%) for 5 min. Under the stream of Ar gas at 80 sccm in a flow rate that was slower than 100 sccm applied for the synthesis of RNTs,[14] the quartz tube was then heated from room temperature to 450 °C. The temperature was increased at a rate of 61 °C/min and maintained at 450 °C for 40 min. The as-prepared products were characterized by using scanning electron microscopy (SEM, XL30S, FEI) and transmission electron microscopy (TEM, CM200, Philips).

Ensemble-Averaged Optical Properties of H_2TPyP-RMTs. Ensemble-averaged optical properties were investigated by measuring UV−vis absorption and photoluminescence spectra of the RMT-dispersed solution or solid mat deposited on quartz glass, using a UV−vis spectrophotometer (Agilent 8453) and spectrofluorometer (Horiba FluoroMax-4) at room temperature. To prepare the solid mat sample, a Si(100) substrate containing as-grown H_2TPyP-RMTs was soaked in water so that the RMTs could be dispersed on the surface of the water. The dispersed RMTs on the water surface were then transferred on cover glass by using a glass pipet, and then the cover glass was naturally dried. In order to remove big crystals or occasionally formed, vertically standing RMTs, a couple of hexane droplets were dropped on the glass substrates and naturally dried.

The PL emission quantum yield (Φ_f) of H_2TPyP-RMTs dispersed in ethylacetate solution was determined by comparing the integrated PL intensity, I_f (the area under the corrected PL spectrum), and the absorbance at the excitation wavelength to the corresponding quantities (I_{sf}) belonging to a solution of a standard compound of known quantum yield (tetraphenyl porphyrin in ethylacetate, $\Phi_{sf} = 0.099$),[21,22]using the following equation, $\Phi_f = (I_f/I_{sf}) \times (A_\lambda/A_{s\lambda}) \times \Phi_{sf}$, where A_λ and $A_{s\lambda}$ are absorbances of the H_2TPyP-RNTs and the standard, respectively.

PL Imaging and Spectral Measurements of Individual H_2TPyP-RMTs. PL imaging and spectral measurements of individual H_2TPyP-RMTs were performed by using CSM-coupled picosecond-time-resolved PL system (Figure S1 in Supporting Information) at room temperature as previously reported.[38] The H_2TPyP-RMTs were coated onto a clean quartz glass by the aforementioned sample preparation method. The RMT-coated quartz glass was mounted on a scanning piezo-electric $X-Y$ stage (Physik Instrumente, P517.3CL), and it was excited through the back of a 100×, 1.3 NA oil immersion objective lens (Carl Zeiss Plan-NEOfluor) by the second harmonic output (410 nm) of self-mode-locked Ti:sapphire laser (Coherent model Mira 900) pumped by a Nd:YVO_4 laser (Coherent Verdi diode pumped laser) (200 fs pulse width with repetition rate of 76 MHz), which was passed through a single mode optical fiber. The excitation power was adjusted by using neutral density filters. The PL signals were collected through an inverted confocal scanning microscope (Carl Zeiss Axiovert 200) equipped with a liquid-nitrogen-cooled intensified charge-coupled device (CCD) detector (Princeton Instruments VersArray) or a polychromator (Acton Research, Spectra Pro 300i) with a CCD camera (Roper Scientific, PI-MAX-1024HG18) for the RMT images and spectral measurement, respectively. The emission was isolated from Rayleigh scattering by a combination of filters: an excitation filter BP 395-440, a dichroic filter FT 460 and an emission filter LP 470 (Carl Zeiss).

The PL emission decay times of a single RMT were measured by time-correlated single photon-counting (TCSPC) system (Edinburgh Instruments) (Figure S1) with time resolution of 20 ps at room temperature. The start signal was collected through the multimode optic fiber from the confocal microscope, and the signal was stopped by synchronization of the Ti:sapphire

laser pulse which was passed through a pulse picker at one-half of the laser repetition rate.

Acknowledgment. This study was supported by MEST (2009-0083200, 2009-0065619, 2008-8-1807, 2007-KRF-C00340, 2010-0002880), EPB center (2009-0063304), Priority Research Centers Program (2009-0094037). H.C.C. thanks the World Class University (WCU) program (R31-2008-000-10059-0). The experimental part of this work is supported by the Creative Research Initiatives (Functional X-ray Imaging) of MEST/KOSEF. We thank to Dr. K. S. Jeon at KRICT for technical support for operation of CSM-coupled PL system.

Supporting Information Available: Layout of confocal scanning microscope (CSM)-coupled spatial and picosecond-time-resolved PL system, and additional PL spectra of H_2TPyP-RMTs with specific excitation pumping power. This material is available free of charge *via* the Internet at http://pubs.acs.org.

REFERENCES AND NOTES

1. Zhao, Y. S.; Fu, H.; Peng, A.; Ma, Y.; Xiao, D.; Yao, J. Low-Dimensional Nanomaterials Based on Small Organic Molecules: Preparation and Optoelectronic Properties. *Adv. Mater.* **2008,** *20*, 2859–2876.
2. Forrest, S. R. The Path to Ubiquitous and Low-Cost Organic Electronic Appliances on Plastic. *Nature* **2004,** *428*, 911–918.
3. Dimitrakopoulos, C. D.; Malenfant, P. R. L. Organic Thin Film Transistors for Large Area Electronics. *Adv. Mater.* **2002,** *14*, 99–117.
4. O'carroll, D.; Lieberwirth, I.; Redmond, G. Microcavity Effects and Optically Pumped Lasing in Single Conjugated Polymer Nanowires. *Nat. Nanotechnol.* **2007,** *2*, 180–184.
5. Zhao, Y. S.; Peng, A.; Fu, H.; Ma, Y.; Yao, J. Nanowire Waveguides and Ultraviolet Lasers Based on Small Organic Molecules. *Adv. Mater.* **2008,** *20*, 1661–1665.
6. Zhao, Y. S.; Xu, J.; Peng, A.; Fu, H.; Ma, Y.; Jiang, L.; Yao, J. Optical Waveguide Based on Crystalline Organic Microtubes and Microrods. *Angew. Chem., Int. Ed.* **2008,** *47*, 7301–7305.
7. Liao, Q.; Fu, H.; Yao, J. Waveguide Modulator by Energy Remote Relay from Binary Organic Crystalline Microtubes. *Adv. Mater.* **2009,** *21*, 4153–4157.
8. Holmes, R. J. Nanowire Lasers Go Organic. *Nat. Nanotechnol.* **2007,** *2*, 141.
9. Rothe, C.; Galbrecht, F.; Sherf, U.; Monkman, A. The β-Phase of Poly(9,9-dioctylfluorene) as a Potential System for Electrically Pumped Organic Lasing. *Adv. Mater.* **2006,** *18*, 2137–2140.
10. Kozlov, V. G.; Bulović, V.; Burrows, P. E.; Forrest, S. R. Laser Action in Organic Semiconductor Waveguideand Double-Heterostructure Devices. *Nature* **1997,** *389*, 362–364.
11. Frolov, S. V.; Shkunov, M.; Vardeny, Z. V.; Yoshino, K. Ring Microlasers from Conducting Polymers. *Phys. Rev. B* **1997,** *56*, R4363–4366.
12. Kadish, K.; Smith, M. K. M.; Guilard, R. *The Porphyrin Handbook*; Academic: San Diego, CA, 2000; Vol 6.
13. Medforth, C. J.; Wang, Z.; Martin, K. E.; Song, Y.; Jacobsen, J. L.; Shelnutt, J. A. Self-Assembled Porphyrin Nanostructures. *Chem. Commun.* **2009,** 7261–7277.
14. Yoon, S. M.; Hwang, I. C.; Kim, K. S.; Choi, H. C. Synthesis of Single-Crystal Tetra(4-pyridyl)porphyrin Rectangular Nanotubes in the Vapor Phase. *Angew. Chem., Int. Ed.* **2009,** *48*, 2506–2509.
15. Yoon, S. M.; Hwang, I. C.; Shin, N.; Ahn, D.; Lee, S. J.; Lee, J. Y.; Choi, H. C. Vaporization−Condensation−Recrystallization Process-Mediated Synthesis of Helical *m*-Aminobenzoic acid Nanobelts. *Langmuir* **2007,** *23*, 11875–11882.
16. Shin, H. S.; Yoon, S. M.; Tang, Q.; Chon, B.; Joo, T.; Choi, H. C. Highly Selective Synthesis of C_{60} Disks on Graphite Substrate by a Vapor−Solid Process. *Angew. Chem., Int. Ed.* **2008,** *47*, 693–696.
17. Yoon, S. M.; Song, H. J.; Hwang, I. C.; Kim, K. S.; Choi, H. C. Single Crystal Structure of Copper Hexadecafluorophthalocyanine (F_{16}CuPc) Ribbon. *Chem. Commun.* **2010,** *46*, 231–233.
18. Yoon, S. M.; Song, H. J.; Choi, H. C. p-Type Semiconducting GeSe Combs by a Vaporization−Condensation−Rcrystallization (VCR) Process. *Adv. Mater.* **2010,** *22*, 2164–2167.
19. Khairutdinov, R. F.; Serpone, N. Photoluminescence and Transient Spectroscopy of Free Base Porphyrin Aggregates. *J. Phys. Chem. B* **1999,** *103*, 761–769.
20. Crosby, G. A.; Demas, J. N. Measurement of Photoluminescence Quantum Yields. Review. *J. Phys. Chem.* **1971,** *75*, 991–1024.
21. Savenkova, N. S.; Kuznetsova, R. T. Spectral and Luminescent Properties of Some Porphyrin Compounds in Different Electronic States. *Opt. Spectrosc.* **2005,** *99*, 751–758.
22. Mekis, A.; Chen, J. C.; Kurland, I.; Fan, S.; Villeneuve, P. R.; Joannopoulos, J. D. High Transmission through Sharp Bends in Photonic Crystal Waveguides. *Phys. Rev. Lett.* **1996,** *77*, 3787–3790.
23. Lin, S. Y.; Chow, E.; Hietala, V.; Villeneuve, P. R.; Joannopoulos, J. D. Experimental Demonstration of Guiding and Bending of Electromagnetic Waves in a Photonic Crystal. *Science* **1998,** *282*, 274–276.
24. Law, M.; Sirbuly, D. J.; Johnson, J. C.; Goldberger, J.; Saykally, R. J.; Yang, P. Nanoribbon Waveguides for Subwevelength Photonics Integration. *Science* **2004,** *305*, 1269–1273.
25. Tong, L.; Gattass, R. R.; Ashcom, J. B.; He, S.; Lou, J.; Shen, M.; Maxwell, I.; Mazur, E. Subwavelength-Diameter Silica Wires for Low-Loss Optical Wave Guiding. *Nature* **2003,** *426*, 816–819.
26. Ohtsu, M.; Hori, H. Near-Field Nano-Optics from Basic Principles to Nano-Fabrication and Nano-Photonics. In *Laser, Photonics, and Electro-Optics Series*; Kogelnik, H., Ed.; Kluwer Academic/Plenum Publishers: New York, 1999; pp 16−30.
27. McGehee, M. D.; Gupta, R.; Veenstra, S.; Miller, E. K.; Díaz-García, M. A.; Heeger, A. J. Amplified Spontaneous Emission from Photopumped Films of a Conjugated Polymer. *Phys. Rev. B* **1998,** *58*, 7035–7039.
28. Malko, A. V.; Mikhailovsky, A. A.; Petruska, M. A. Hollingsworth, J. A.; Htoon, H.; Bawendi, M. G.; Klimov, V. I. From Amplified Spontaneous Emission to Microring Lasing Using Nanocrystal Quantum Dot Solids. *Appl. Phys. Lett.* **2002,** *81*, 1303–1305.
29. Tsuboi, T.; Wasai, Y.; Nabatova-Gabain, N. Optical Constants of Platinum Octaethyl Porphyrin in Single-Layer Organic Light Emitting Diode Studied by Spectroscopic Ellipsometry. *Thin Solid Films* **2006,** *496*, 674–678.
30. Yan, H.; Johnson, J.; Law, M.; He, R.; Knutsen, K.; McKinney, J. R.; Pham, J.; Saykally, R.; Yang, P. ZnO Nanoribbon Microcavity Lasers. *Adv. Mater.* **2003,** *15*, 1907–1911.
31. Batrak, D. V.; Bogatov, A. P.; Drakin, A. E.; D'yachkov, N. V.; Miftakhutdinov, D. R. Modes of a Semiconductor Rectangular Microcavity. *Quant. Electron.* **2008,** *38*, 16–22.
32. Wu, J. H.; Liu, A. Q. Exact Solution of Resonant Modes in a Rectangular Resonator. *Opt. Lett.* **2006,** *31*, 1720–1722.
33. Barrelet, C. J.; Greytak, A. B.; Lieber, C. M. Nanowire Photonic Circuit Element. *Nano Lett.* **2004,** *4*, 1981–1985.
34. Voss, T.; Svacha, G. T.; Mazur, E.; Müller, S.; Ronning, C.; Konjhodzic, D.; Marlow, F. High-Order Waveguide Modes in ZnO Nanowires. *Nano Lett.* **2007,** *7*, 3675.
35. Carlucci, L.; Ciani, G.; Proserpio, D. M.; Porta, F. Open Network Architectures from the Self-Assembly of $AgNO_3$ and 5,10,15,20-Tetra(4-pyridyl)porphyrin (H_2tpyp) Building Blocks: The Exceptional Self-Penetrating Topology of the 3D Network of $[Ag_8(Zn^{II}tpyp)_7(H_2O)_2](NO_3)_8$. *Angew. Chem., Int. Ed.* **2003,** *42*, 317–322.
36. Li, L. L.; Yang, C. J.; Chen, W. H.; Lin, K. J. Towards the Development of Electrical Conduction and Lithium-Ion Transport in a Tetragonal Porphyrin Wire. *Angew. Chem., Int. Ed.* **2003,** *42*, 1505–1508.
37. Sun, D.; Tham, F. S.; Reed, C. A.; Boyd, P. D. W. Extending Supramolecular Fullerene-Porphyrin Chemistry to Pillared Metal-Organic Frameworks. *Proc. Natl. Acad. Sci. U.S.A.* **2002,** *99*, 5088–5092.
38. Lee, J.; Yoon, M. Synthesis of Visible Light-Sensitive ZnO Nanostructures: Subwavelength Waveguides. *J. Phys. Chem. C* **2009,** *113*, 11952–11958.